Journal of Sound and Vibration (1998) **211**(5), 801–818

IMPACT RESPONSE AND THE INFLUENCE OF FRICTION

C. J. Begley and L. N. Virgin

Department of Mechanical Engineering and Materials Science, Duke University, Durham, North Carolina 27708-0300, *U.S.A.*

(*Received* 20 *October* 1997)

Non-smooth stiffness and damping characteristics are commonly encountered in mechanical systems. The specific physical contacts considered in this paper are impact and friction. Although these individual effects have been the subject of quite intensive research it is their interaction and influence on the dynamic behavior of a mechanical oscillatory system that is the subject of the current work. Dynamical systems theory is used as a conceptual framework and comparisons are made between numerical and experimental results over a relatively wide range of parameters.

1. INTRODUCTION

Motion-limiting constraints including impacting and sticking are thoroughly non-linear effects. Impact oscillators have been the focus of a number of studies, due in part to the variety of practical applications for which an impact model is appropriate, and also due to the considerable intrigue provided by these systems from a dynamical systems perspective. Friction, though also present and potentially significant in many of the impact applications, represents further complexity but has often been neglected.

For a single-degree-of-freedom system, two-sided impact implies that the amplitude of motion is bounded in either direction. Shaw [1] described the local and global bifurcation structure of this type of system for a given parameter range. The qualitative flavor of Shaw's work is well reflected below, particularly for low friction levels. Additional two-sided impact studies were performed by Li *et al*. [2], who considered a zero-stiffness impact oscillator intended to mimic the behavior of pin joints in space structures. Shaw and Rand [3] analyzed the behavior of an inverted pendulum, constrained on either side, which resulted in a system with negative stiffness. Thompson and Ghaffari [4] conducted some numerical experiments on a simple impact oscillator showing some interesting scaling behavior and the onset of chaos. Many other studies have been conducted on systems with discontinuities in their stiffness characteristics [5–20].

Dry friction has been the subject of many investigations over the years. A basic, and certainly not exhaustive, sample is contained in references [21–42]. It has also been included in a limited number of impact studies. Mansour and Filho [43], and later Bapat [44], included the effects of friction in examining the response of impact dampers. An impact damper consists of a loose (secondary) mass that slides inside of a container, which is attached to the primary mass. The loose mass impacts the sides of the container, dissipating energy and reducing the amplitude of vibration of the primary mass. Whiston [45] considered an impact oscillator that moves in two-dimensional space in response to elliptical harmonic excitation. In order to facilitate wear calculations, the system includes

0022–460X/98/150801 + 18 $25.00/0/sv971389

Coulomb friction as the oscillating mass slides along either of two impact surfaces. And Glocker and Pfeiffer [46] accounted for the possibility of friction forces in their analysis of a percussive drilling machine. Finally, the work of Cone and Zadoks [47] in particular considered the combined effects of friction and two-sided impact in terms of dynamical systems theory. The base-excited system and relatively large friction force are employed to reflect the behavior of a loose bolt in a vibratory environment.

Experimental work on impact oscillators includes several studies on single-sided impact [18, 48–50], relatively fewer on two-sided impact [49, 51], and Hinrichs *et al*. [52] discuss both the effects of friction and impact in experimental systems. The present work includes frictional damping in an extensive study of a two-sided impact oscillator, both in simulation and experiment. It is demonstrated that a relatively simple experiment exhibits the spectrum of non-linear features observed in, and predicted by the mathematical model.

2. THE PHYSICAL SYSTEM

Consider a single-degree-of-freedom oscillator consisting of a rotational inertia, harmonically forced through a base spring, and subject to impact at the critical angles ϕ_L and ϕ_R, as shown in Figure 1(a). Friction is assumed to be present at the pivot. For small ϕ, a summation of moments about the pivot provides the equation of motion:

$$I\ddot{\phi} + cL_s^2\,\dot{\phi} + kL_s^2\,\phi + L_f\,F(\dot{\phi}) + L_i\,G(\phi) = cL_s\,\dot{y} + kL_s\,y, \tag{1}$$

where $F(\dot{\phi})$ and $G(\phi)$ represent non-linear forces due to friction and impact respectively and are considered in more detail later, together with an experimental realization of such a system. The base forcing is harmonic at frequency ω and amplitude $Y_0 : y(t) = Y_0 \sin(\omega t)$.

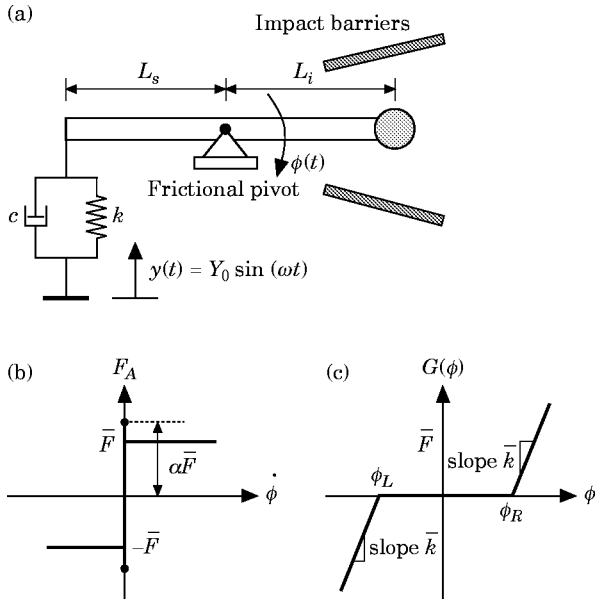

Figure 1. (a) Schematic of impact/friction oscillator, (b) piecewise linear friction model, (c) trilinear impact model.

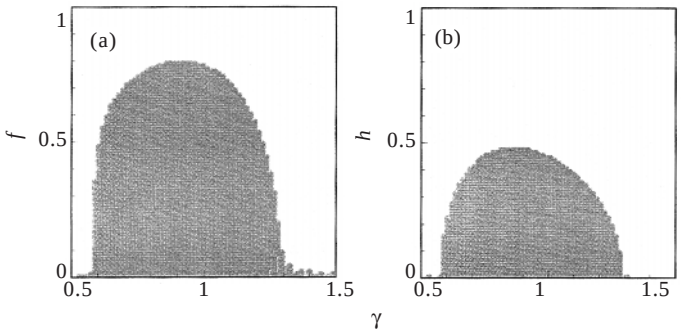

Figure 2. Damping and frequency combinations for which response amplitude exceeds critical baseline value ($|\theta_{max}| > 1{\cdot}5$); (a) friction damping; (b) viscous damping.

2.1. FRICTION MODELLING

The modelling of friction is an extremely difficult task, influenced as it is by a myriad of different factors, and has been the subject of comprehensive study [25, 30, 37, 40]. Included in the list of contributary factors are area of contact, surface finish, lubrication, normal load, damage or wear, temperature and humidity. The interactive effects of friction forces and system dynamics may be intricate including the possibility of "frictional memory" [25]. For the purposes of the current study (where the global dynamics effects of friction are of primary concern) a relatively simple friction law is adopted. A piece-wise linear Coulomb friction relationship can be written as

$$F_A(\dot{\phi}) = \bar{F}\,\mathrm{sgn}(\dot{\phi}), \qquad \text{for } \dot{\phi} \neq 0, \qquad -\alpha\bar{F} \leqslant F_A(\dot{\phi}) \leqslant \alpha\bar{F}, \qquad \text{for } \dot{\phi} = 0. \tag{2}$$

where the parameter α accounts for a static friction level that differs from kinetic friction. A schematic picture of this model is shown in Figure 1(b).

2.2. IMPACT MODELLING

The modelling of impact is somewhat more straightforward than friction although there are again a number of choices to be made. A simple coefficient of restitution has been shown to work well in related studies [16]. However, since the current study involves a rubber ball contacting a flat metal surface there is a finite contact time and hence a change of stiffness model is used here where the equation of motion switches (at impact) to one with a much higher (but still linear) stiffness, i.e., a trilinear stiffness [12, 53, 54]. This characteristic is described mathematically as

$$G(\phi) = \begin{Bmatrix} \bar{k}L_i(\phi - \phi_R), & \phi > \phi_R, \\ 0, & \phi_L \leqslant \phi \leqslant \phi_R, \\ \bar{k}L_i(\phi - \phi_L), & \phi < \phi_L, \end{Bmatrix} \tag{3}$$

and is also shown schematically in Figure 1(c). Here, the contact stiffness is $\bar{k}$ at the right and left boundaries ϕ_L and ϕ_R.

3. NON-DIMENSIONALIZATION

It is convenient to reduce the number of parameters in the equation of motion. Time is normalized with respect to the primary natural frequency of the system, ω_n. A non-dimensional co-ordinate, $\theta(\tau)$, and several non-dimensional parameters are defined:

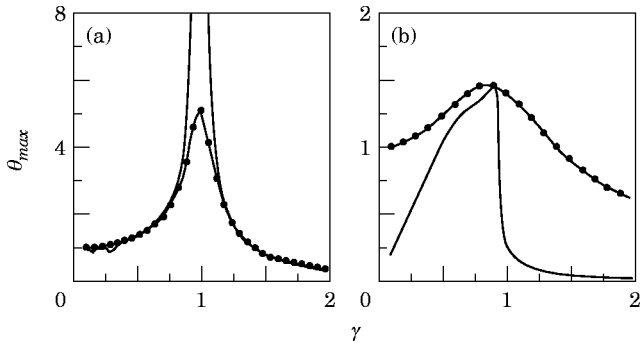

Figure 3. Response spectra for friction system (——) and viscous system (·—·): (a) $h = 0{\cdot}1$, $f = 0{\cdot}15$; (b) $h = 0{\cdot}5$, $f = 0{\cdot}8$.

$$\omega_n = \sqrt{kL_s^2/I}, \qquad \tau = \omega_n t, \qquad \theta(\tau) = \phi(t)L_s/Y_0, \qquad \gamma = \omega/\omega_n,$$
$$h = cL_s/2I\omega_n, \qquad \bar{\omega}_n = \sqrt{\bar{k}L_i^2/I}, \qquad f = \bar{F}L_f/L_s\,Y_0\,k,$$
$$\dot{\theta}_c(\tau) = \dot{\phi}_c(t)L_s/\omega_n\,Y_0, \qquad \rho = \bar{\omega}_n/\omega_n = \sqrt{\bar{k}L_i^2/kL_s^2}, \qquad \sigma_{R,L} = \phi_{R,L}\,L_s/Y_0. \tag{4}$$

Now, rescaling the equation of motion (1) and incorporating the friction and impact models (equations 2 and 3), and using the above non-dimensionalization leads to

$$\ddot{\theta} + 2h\dot{\theta} + \theta + f(\dot{\theta}) + g(\theta) = 2h\gamma\cos(\gamma\tau) + \sin(\gamma\tau), \tag{5}$$

where

$$f(\dot{\theta}) = \alpha f\,\mathrm{sgn}(\dot{\theta}), \qquad \dot{\theta} \neq 0, \qquad -f \leqslant f(\dot{\theta}) \leqslant f, \qquad \dot{\theta} = 0, \tag{6}$$

and

$$g(\theta) = \begin{Bmatrix} \rho^2(\theta - \sigma_R), & \theta > \sigma_R, \\ 0, & \sigma_L \leqslant \theta \leqslant \sigma_R, \\ \rho^2(\theta + \sigma_L), & \theta < \sigma_L. \end{Bmatrix} \tag{7}$$

The resulting parameters of interest are the ratio of the driving frequency to natural frequency, γ, the normalized friction force, f, the viscous damping ratio, h, the left and right impact locations, σ_L and σ_R, and the impact-to-free stiffness ratio, ρ. The friction force has been normalized in such a way that it is equivalent to half of the static equilibrium range in non-dimensional co-ordinates. That is, $f = [(\theta_e)_{\max} - (\theta_e)_{\min}]/2$, where θ_e represents

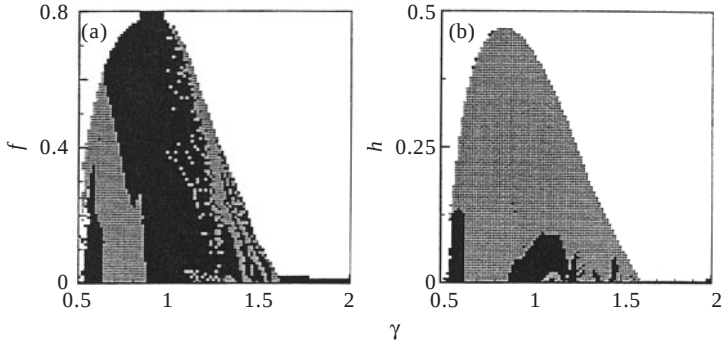

Figure 4. Periodicity charts for symmetric impact, $\sigma = \pm 1{\cdot}5$: (a) friction system; (b) viscous system.

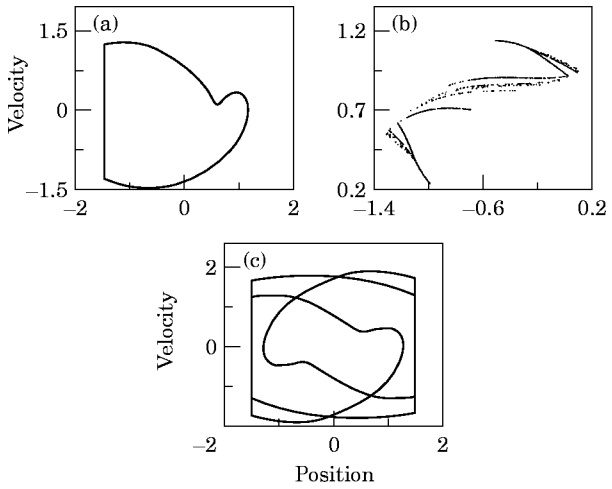

Figure 5. Typical responses of symmetric system: (a) single-impact phase projection; (b) Poincaré section showing a chaotic attractor; (c) period-3 phase projection.

an angle of equilibrium in the presence of friction. This is convenient for experimental purposes because the friction force can be estimated directly from a simple measurement of the static equilibrium range without prior knowledge of the coefficient of friction or spring force. In fact, the total friction force as contributed by all frictional interfaces in the system is assessed with one measurement. The impact locations provide similar interpretations due to this normalization method. Because the forcing amplitude, Y_0, is part of the conversion factor in going to normalized co-ordinates, the amplitude of the response as forcing frequency approaches zero is equal to unity. So, an impact location of $\sigma = 2{\cdot}0$ means that the impact wall is twice as far from equilibrium as the "static" deflection due to Y_0. Likewise, $\sigma < 1{\cdot}0$ indicates that impact cannot be avoided at low frequencies.

4. SOLVING FOR THE MOTION

It is well known that traditional numerical integration techniques, such as Runge–Kutta, must be used with some caution when applied to systems that are piecewise linear, i.e., the location of the exact transition point between linear sub-intervals is important [55]. However, a number of approaches have been developed which take advantage of the exact linear solution over a sub-region of the motion, and a solution can be pieced together by matching [9]. Another popular pseudo-analytical technique is based on the imposition of certain periodicity and boundary conditions [12], but is limited to periodic motion. In the current study a numerical technique is used which takes advantage of the linearity of the inter-impact region.

5. EFFECTS OF DAMPING AND IMPACT LOCATION

Dry friction is a dissipative force that is often replaced in an analysis by an "equivalent" linear viscous damping in order to simplify the governing equations. Yet, it is difficult to define an "equivalent" damping level because friction itself is a non-linear phenomenon that can produce qualitative effects not possible in a linear oscillator. As Klepp [56] and others have concluded, it is not feasible to define a single equivalent viscous damping level

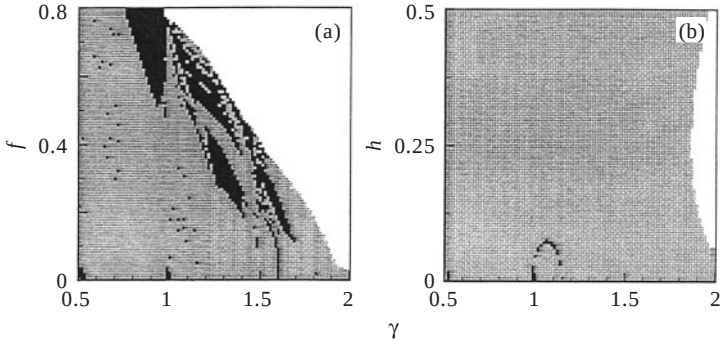

Figure 6. Periodicity charts for symmetric impact, $\sigma = \pm 0{\cdot}8$: (a) friction system; (b) viscous system.

to replace friction damping and still retain satisfactory correlation between all system response characteristics over a significant range of forcing frequencies. At a given forcing frequency, however, it is possible to locate damping levels that produce identical measures of a single response attribute, such as amplitude, energy dissipated per cycle, or length of transient.

Though defining universally equivalent damping levels is not realistic, endeavoring to compare the effects of the two types of damping requires at least the choice of a scaling factor to promote an approximately "apple to apples" study. From a non-linear dynamics perspective, a primary concern is the location of bifurcation phenomena and the range of frequencies over which irregular behavior occurs. For impacting systems, the dominant bifurcations occur near so-called grazing orbits, or transitions between non-impacting and impacting solutions. It seems natural, then, to include the relationship between response amplitude and impact amplitude in the computation of the scaling factor.

In Figure 2, a baseline impact location of $\sigma = \pm 1{\cdot}5$ is chosen. Friction and forcing frequency combinations that lead to steady state response amplitudes that exceed the impact amplitude ($|\theta_{\max}| > 1{\cdot}5$) are then plotted in gray in Figure 2(a). An identical interpretation is made for the (linear) viscously damped system in Figure 2(b). The similar shapes of the shaded regions and the maximum damping levels required to prevent impact near resonance point to the logical choice of a rough scaling factor for this case: the maximum $f = 0{\cdot}8$ is deemed comparable to $h = 0{\cdot}5$. The damping ranges displayed in the "periodicity charts" presented below reflect this scaling derivation.

To demonstrate the fact that "equivalent" damping is not an accurate description over the entire frequency range of interest, Figure 3 shows the response spectra for low

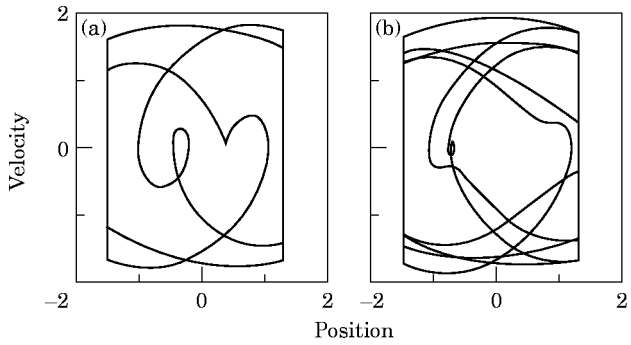

Figure 7. Phase projections: (a) period-3 motion; (b) period-6 motion.

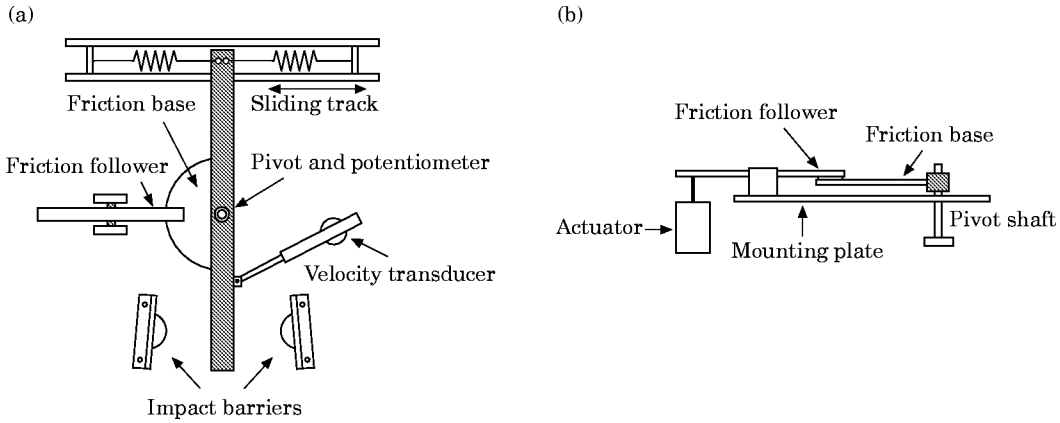

Figure 8. (a) Schematic of the experimental rig (overhead view), (b) friction mechanism (side view), impact barriers and measuring equipment not shown.

(Figure 3(a)) and high (Figure 3(b)) levels of damping, in the absence of impact barriers. At low damping, friction is unable to attenuate the large response amplitude near resonance. High damping levels reveal two important points: the amplitude of response for the frictional system dips well below the linear response amplitude at low frequencies, and the transition from large to small amplitudes immediately following resonance is abrupt for the frictional system. These facts help to explain some of the trends noted in the periodicity charts below.

5.1. EXPLANATION OF "PERIODICITY" CHARTS

The shaded figures below compare the effects of frictional and viscous damping by comparing the period of the response (normalized with respect to the forcing period) that results for the indicated system parameters, in response to quiescent initial conditions, after 200 forcing cycles. These figures are essentially two-dimensional bifurcation diagrams, using 'zero' initial conditions for each set of parameters. A small amount of viscous damping ($h = 0{\cdot}001$) is included for the friction cases to facilitate numerical convergence, particularly near resonance. For all viscous cases, $f = 0{\cdot}0$. The shading code is: *white*: period-1, non-impacting solutions. For the viscous damping cases, white represents entirely linear response. *gray*: period-1 solutions that include at least one impact per cycle. *black*: higher order periodic solutions and chaos.

It should be noted that the periodicity charts are constructed for a single choice of initial conditions and therefore do not provide competing solution information. Further details of competing basins of attraction for this system can be found in Virgin *et al*. [57].

5.2. SYMMETRIC IMPACT

A typical case where the impact barriers are positioned symmetrically with respect to the natural equilibrium of the oscillator is presented in Figure 4. For $\sigma = \pm 1{\cdot}5$, higher-order periodic and potentially chaotic response are more prevalent for the friction oscillator, particularly at higher damping levels. It is interesting that an *increase* in friction is likely to lead to higher order behavior in many cases. Period-1 solutions dominate for viscous damping. Examples of specific friction-damped response are shown in Figure 5. The period-1 solution that impacts only the left barrier (Figure 5(a)) has an anti-symmetric partner solution (not shown) for the same parameter set. The chaotic attractor shown in Figure 5(b) was not observed in the viscous system at comparable damping levels. Finally,

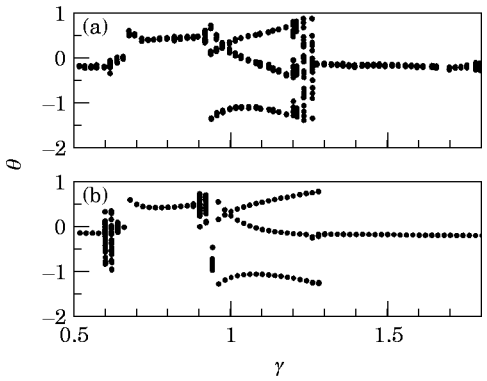

Figure 9. Bifurcation diagrams for symmetric impact ($\sigma = \pm 1{\cdot}6$) and low friction ($f = 0{\cdot}05$): (a) experiment; (b) simulation.

a period-3 motion (Figures 5(c)) is dominant in both systems for low damping levels. In fact, the low damping level results across the entire frequency range are very similar for the two systems, as might be expected.

When the impact amplitude is reduced to $\sigma = \pm 0{\cdot}8$, period-1 impacting solutions (gray) dominate for both systems, as shown in Figure 6. By recalling that for $\sigma < 1$ the impact locations are closer to equilibrium than the maximum base excitation displacement, implying that the linear (viscous) system cannot avoid impact at the lower frequencies, where the linear response amplitude asymptotes to $\theta_{\max} = 1{\cdot}0$, independently of damping level. Interestingly, friction is capable of preventing impact as the forcing frequency approaches zero, even for $\sigma < 1$, due to a response amplitude scaling [53]. For the range of frequencies considered here, however, impact is not avoided in either system until higher frequencies. Referring back to Figure 3, the abrupt drop in response amplitude for high friction levels helps to explain why the friction system shows a larger (white) region of non-impacting response in Figure 6.

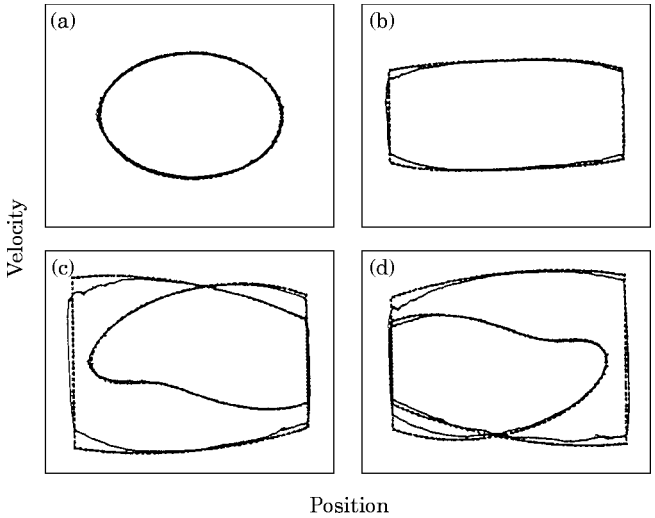

Figure 10. Coexisting attractors at $\gamma = 1{\cdot}338$: (a) non-impact response; (b) double-impact response; (c and d) anti-symmetric period-2 response.

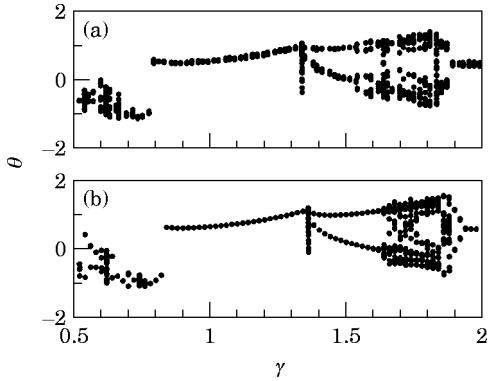

Figure 11. Bifurcation diagrams for asymmetric impact ($\sigma = -1{\cdot}1,\ 2{\cdot}2$) and low friction ($f = 0{\cdot}05$): (a) experiment; (b) simulation.

5.3. ASYMMETRIC IMPACT

Given the critical $\sigma = 1$ boundary, a representative case of asymmetric impact is chosen, i.e., $\sigma_L = -1{\cdot}5$, $\sigma_R = 1{\cdot}3$. Figure 7 shows a period-3 and period-6 solution. For other asymmetric impact locations it is also possible to obtain periodic orbits that impact each side a different number of times.

5.4. GENERAL TRENDS AND DISCUSSION

Though the friction-damped system is prone to more extensive higher order response regions, the qualitative nature of the response for regions of matching shade is generally consistent between systems. Non-impacting solutions are more common in the friction system. The quiescent initial conditions are apt to encourage the non-impacting solutions for both systems, especially for higher frequencies. However, non-zero initial conditions ($\theta_0 = 1{\cdot}0$, $\dot{\theta}_0 = 1{\cdot}0$) were examined for the symmetric $\sigma = \pm 1{\cdot}5$ case, with surprisingly little overall effect. Much of the non-impacting (white) regions at higher frequencies became coexisting period-1 impacting (gray) motion as a result of the higher energy initial conditions, but little change was observed elsewhere, for either type of damping. The effect of allowing fewer transient cycles before recording the periodicity of the behavior was also

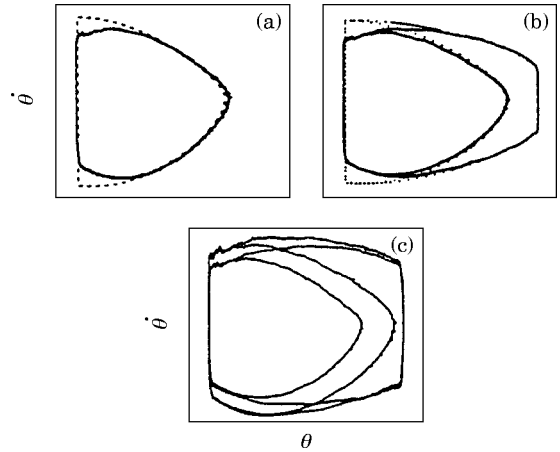

Figure 12. Phase projections for experiment (——) and simulation (----): (a) single impact response, $\gamma = 1{\cdot}12$; (b) period-2 motion, $\gamma = 1{\cdot}41$; (c) period-4 motion, experiment only, $\gamma = 1{\cdot}58$.

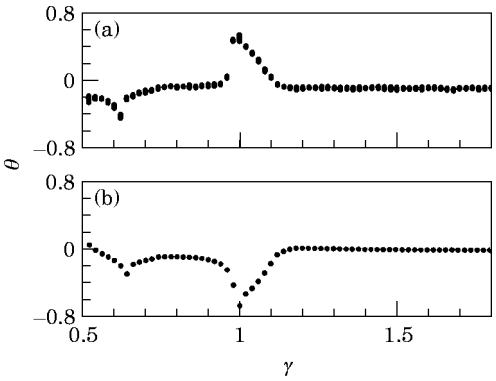

Figure 13. Bifurcation diagrams for symmetric impact ($\sigma = \pm 0{\cdot}8$) and low friction ($f = 0{\cdot}04$): (a) experiment; (b) simulation.

found to be minimal. It was speculated that one or the other of the systems may be more effective at reducing the length of transients (again starting from zero initial conditions.) This proved not to be the case, as the primary effect of allowing only ten transient cycles was to produce more non-convergent response across the lower damping range, roughly equivalently for both forms of damping.

6. EXPERIMENTAL SETUP

An experimental system was constructed to examine the combined effects of impact and friction analogous to the theoretical model described above. A schematic is shown in Figure 8. A more complete description can be found in Begley [58]. Independent position and velocity measurements are made using a potentiometer at the pivot and a linear velocity transducer, respectively. In this case there is, therefore, no need for phase space reconstruction based on time lag embedding. Their signals are then filtered using 100 Hz low pass analog filters. The friction force can be adjusted by means of a stationary friction lever, which is also shown in Figure 8. Impact walls with rubber stoppers are located on

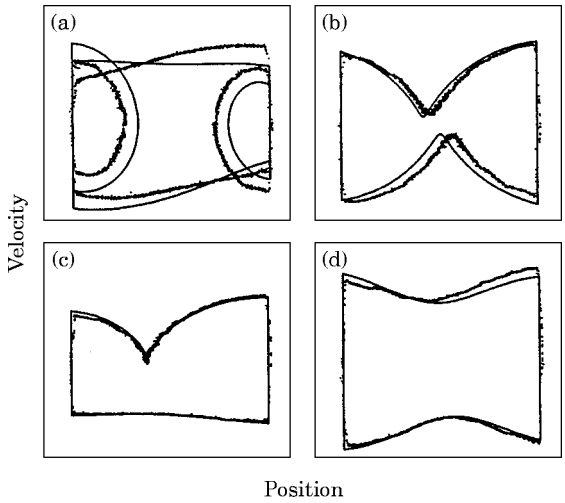

Figure 14. Phase projections for experiment (heavy line) and simulation (thin line): (a) $\gamma = 0{\cdot}54$; (b) $\gamma = 0{\cdot}8$; (c) $\gamma = 1{\cdot}1$; (d) $\gamma = 1{\cdot}4$.

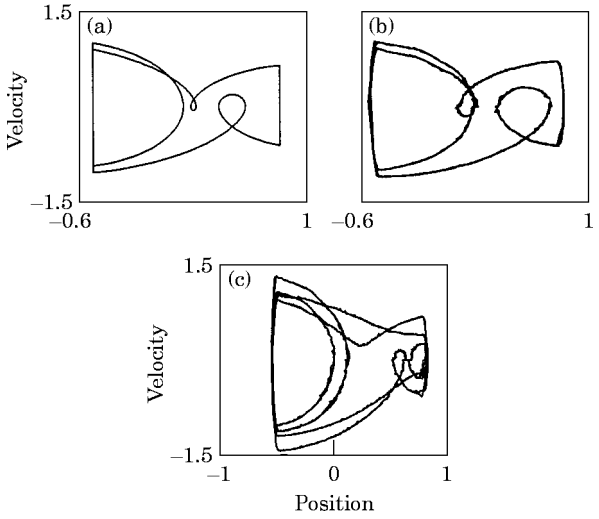

Figure 15. Phase projections: (a) simulation, $\gamma = 0{\cdot}54$; (b) experiment, $\gamma = 0{\cdot}54$; (c) experiment, $\gamma = 0{\cdot}61$.

either side of the natural equilibrium of the system. The location of these impact bumpers is also adjustable via radial grooves cut in the mounting plate. The oscillating mass itself is made of aluminum stock ($2{\cdot}2 \times 1{\cdot}6 \times 31$ cm), with a steel shaft supported by radial bearings in two locations along its length.

The sliding track depicted in Figure 8 provides sinusoidal base excitation. The track itself is driven by a "scotch yoke" mechanism that transforms the rotational motion of a drive motor into the linear harmonic motion of the track. The available driving frequency range is 0–2 Hz; amplitude range of roughly 2–10 cm. A flywheel and drive belts are positioned between the drive motor and scotch yoke mechanism to smooth the motion. Attached to the flywheel is a magnetic sensor (modified Reed relay) that can detect the zero position (or other arbitrary position) of the forcing mechanism once per cycle. This provides a means to perform experimental Poincaré sections.

Many of the non-dimensional parameters could be measured directly from the rig. The natural frequency was estimated to be approximately 0·9 Hz via free response data. This value is then related to the known driving frequency to calculate γ. The friction level was computed (αF) by measuring the range of static equilibria for several track positions and

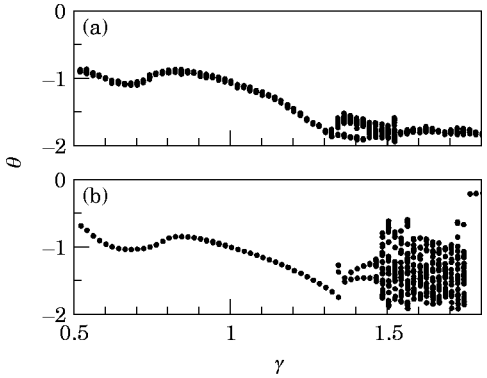

Figure 16. Bifurcation diagrams for asymmetric impact ($\sigma = -1{\cdot}91, 1{\cdot}08$) and high friction ($f = 0{\cdot}38$): (a) experiment; (b) simulation.

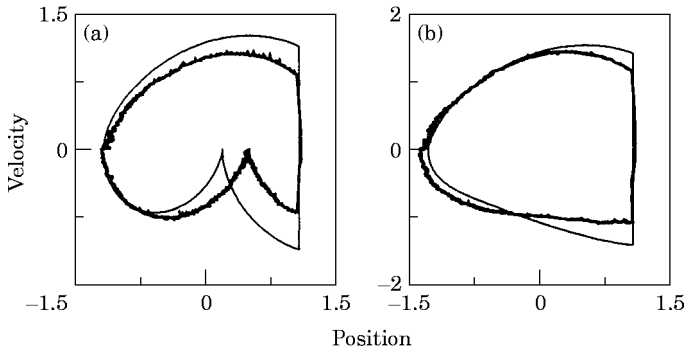

Figure 17. Phase projections for experiment (heavy line) and simulation (thin line): (a) $\gamma = 0{\cdot}7$; (b) $\gamma = 1{\cdot}1$.

averaging over a number of measurements. As a check on the estimate of viscous damping and friction present in the system, a method recently proposed by Feeny and Liang [59] was used. Using their technique the levels were estimated at $f = 0{\cdot}057$ and $h = 0{\cdot}024$, which compared with estimates from the static equilibria range of $f = 0{\cdot}05$ and $h = 0{\cdot}02$.

A related study by the same authors [53] focuses attention specifically on friction modelling and measurement.

7. EXPERIMENTAL RESULTS

A catalog of experimental friction–impact results is presented in the following section. These results include bifurcation diagrams and phase trajectories for symmetric and asymmetric impact locations, $\sigma > 1{\cdot}0$ and $\sigma < 1{\cdot}0$, and high and low levels of friction. The experimental data is compared to simulation results where possible, using the experimentally measured parameters. The figure captions include the pertinent parameter information. In the bifurcation diagrams for the experimental results (e.g. Figure 9(a)) the irregular frequency intervals reflect a lack of *a priori* setting for the frequency rather than uncertainty in the value of the frequency. Since the experimental results are rather extensive a list of some key details is presented.

In Figure 10, four co-existing attractors were located at $\gamma = 1{\cdot}338$, both experimentally and in simulation.

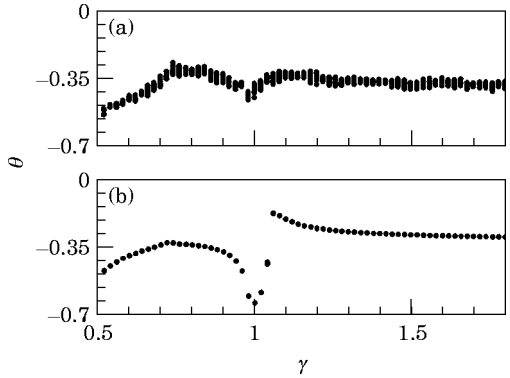

Figure 18. Bifurcation diagrams for symmetric impact ($\sigma = \pm 0{\cdot}8$) and high friction ($f = 0{\cdot}36$): (a) experiment; (b) simulation.

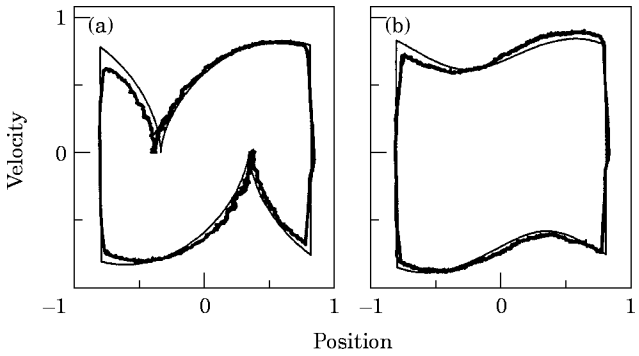

Figure 19. Phase projections for experiment (heavy line) and simulation (thin line): (a) $\gamma = 0{\cdot}7$; (b) $\gamma = 1{\cdot}4$.

Experimental results in Figures 11 and 12 reveal a significant period-4 branch (around $\gamma = 1{\cdot}6$) that is not seen in the simulation results.

The bifurcation diagrams in Figure 13 indicate that the experiment and simulation choose different anti-symmetric branches near $\gamma = 1{\cdot}0$. Both antisymmetric solutions were recorded for experiment and simulation; an example of one response is shown in Figure 14(c).

Figure 15 indicates a period-1 solution that impacts twice on the left wall, once on the right wall per cycle. This response experiences period doubling in experiment only, Figure 15(c).

Significant single impact response branches were recorded for the largely asymmetric system, Figures 16 and 17.

Double impact period-1 responses dominate the small impact, high friction case, Figures 18 and 19.

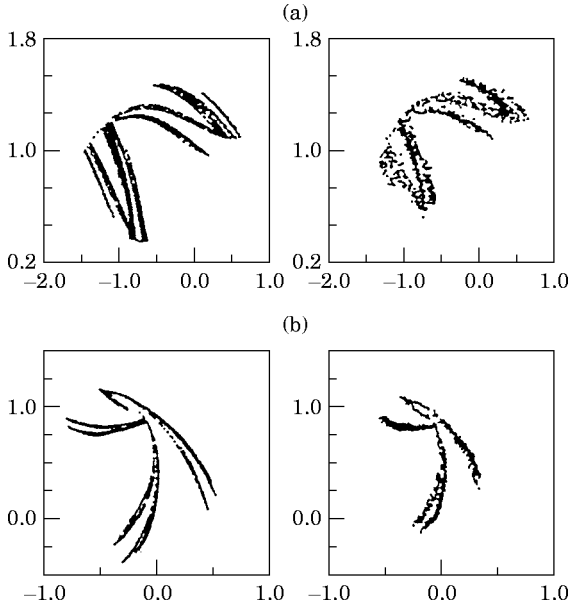

Figure 20. Examples of chaotic attractors, simulation (left) and experiment (right): (a) $\gamma = 0{\cdot}88$, $\sigma = (-1{\cdot}86, 1{\cdot}75)$, $f = 0{\cdot}06$; (b) $\gamma = 0{\cdot}58$, $\sigma = (-1{\cdot}53, 1{\cdot}47)$, $f = 0{\cdot}04$.

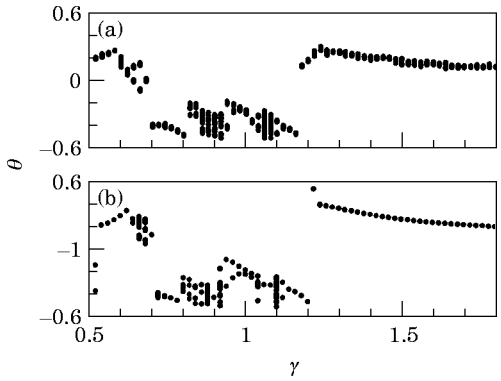

Figure 21. Bifurcation diagrams for asymmetric impact ($\sigma = -0{\cdot}51, 0{\cdot}82$) and low friction ($f = 0{\cdot}04$): (a) experiment; (b) simulation.

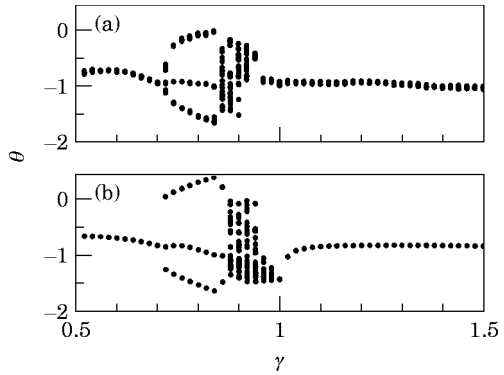

Figure 22. Bifurcation diagrams for symmetric impact ($\sigma = \pm 1{\cdot}93$) and high friction ($f = 0{\cdot}33$): (a) experiment; (b) simulation.

The chaotic attractor "fingers" in Figure 20 are typical of this system. Some sharpness in the detail of the attractor is lost in the experimental results due to noise.

For the most part, the correlation between simulation and experiment is excellent. The bifurcation diagrams in particular reveal qualitative agreement over the entire range of

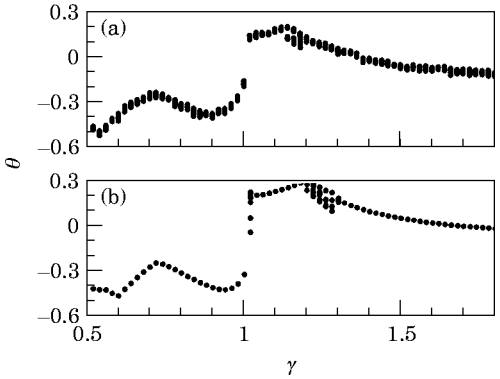

Figure 23. Bifurcation diagrams for asymmetric impact ($\sigma = -0{\cdot}51, 0{\cdot}82$) and high friction ($f = 0{\cdot}34$): (a) experiment; (b) simulation.

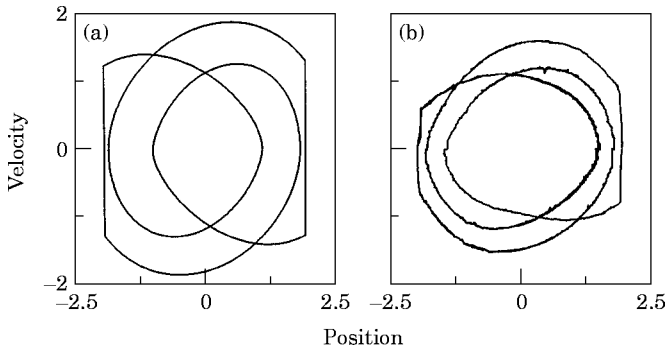

Figure 24. Period-3 motion, $\gamma = 0{\cdot}8$: (a) simulation; (b) experiment.

forcing frequencies (see also Figures 21–23). Higher friction levels produce bifurcation frequencies to match simulation as well. Subtle differences are observed in the amount of detail included in the experimental results, which is not unexpected. For instance, the amplitude and frequency range of the multi-periodic response seen in Figure 16 is not as extensive in experiment as in simulation. In certain phase projections, such as Figure 12, the experimentally measured impact velocities are not as large as the simulation predicts. This may be partially due to the 100 Hz low pass analog filters that are used on the position and velocity traces. Also, the experimental results tend to produce a high frequency "ringing" immediately after impact that could be a result of the vibration of the measuring equipment itself at impact. Again, this effect is neither unexpected, nor entirely avoidable. In general, the experimental system was able to produce very satisfying impact results that confirm many of the trends noted in the periodicity charts presented above (see also Figures 24 and 25).

A more recent type of non-linear feature relevant to this type of system is the occurrence of grazing bifurcations [60–62]. A description of the geometry of these types of low-velocity impacts and their relationship with basin boundaries will form the basis of a subsequent study [54].

8. SUMMARY

Impact and friction oscillators have received considerable attention over recent years. This study has highlighted the effect of *both* motion constraints and Coulomb friction

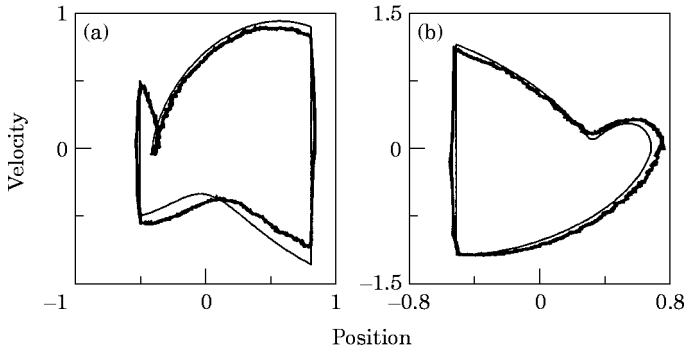

Figure 25. Phase projections for experiment (heavy line) and simulation (thin line): (a) $\gamma = 0{\cdot}9$; (b) $\gamma = 1{\cdot}1$.

(making the system piecewise linear in both its force–position and force–velocity characteristics). In the absence of both friction and impact this system is linear, and hence effective comparsions were made to the baseline case. The forcing frequency and forcing amplitude were the main control parameters although the impact locations were also adjusted and thus highlighted the role of asymmetries in the response. The levels of friction were chosen in relation to the viscous damping present in the system, and it is worth pointing out that most of the responses illustrated in this paper were quite robust, i.e., they appeared over a relatively wide range of parameters. The range and variety of both periodic and chaotic responses (sometimes co-existing) was extensive. This study will thus provide a foundation for further study, including basins of attraction and control. Some modelling issues were discussed for these highly non-linear systems but the key emphasis was placed on a qualitative correlation between simulation and experiment. Very good agreement was achieved.

REFERENCES

1. S. W. Shaw, 1985 *Journal of Applied Mechanics* **52**, 453–464. The dynamics of a harmonically excited system having rigid amplitude constraints, parts 1 and 2.
2. G. X. Li, R. H. Rand and F. C. Moon 1990 *International Journal of Non-linear Mechanics* **25**, 417–432. Bifurcations and chaos in a forced zero-stiffness oscillator.
3. S. W. Shaw and R. H. Rand 1989 *International Journal of Non-Linear Mechanics* **24**, 41–56. The transition to chaos in a simple mechanical system.
4. J. M. T. Thompson and R. Ghaffari 1982 *Physics Letters* **91A**, 5–8. Chaos after period-doubling bifurcations in the resonance of an impact oscillator.
5. G. S. Whiston 1979 *Journal of Sound and Vibration* **67**, 179–186. Impacting under harmonic excitation.
6. G. S. Whiston 1987 *Journal of Sound and Vibration* **115**, 303–319. The vibro-impact response of a harmonically excited and preloaded one-dimensional linear oscillator.
7. G. S. Whiston 1987 *Journal of Sound and Vibration* **118**, 395–429. Global dynamics of a vibro-impacting linear oscillator.
8. G. S. Whiston 1992 *Journal of Sound and Vibration* **152**, 427–460. Singularities in vibro-impact dynamics.
9. S. W. Shaw and P. J. Holmes 1983 *Journal of Sound and Vibration* **90**, 129–155. A periodically forced piecewise linear oscillator.
10. S. W. Shaw and P. J. Holmes 1983 *Journal of Applied Mechanics* **50**, 849–857. A periodically forced impact oscillator with large dissipation.
11. G. R. Tomlinson and J. Lam 1984 *Journal of Sound and Vibration* **96**, 111–125. Frequency response characteristics of structures with single and multiple clearance-type non-linearity.
12. S. Natsiavas 1989 *Journal of Sound and Vibration* **134**, 315–331. Periodic response and stability of oscillators with symmetric trilinear restoring force.
13. S. Natsiavas 1990 *Journal of Sound and Vibration* **141**, 97–102. Stability and bifurcation analysis for oscillators with motion limiting constraints.
14. Y. B. Kim and S. T. Noah 1991 *Journal of Applied Mechanics* **58**, 545–553. Stability and bifurcation analysis of oscillators with piecewise-linear characteristics: a general approach.
15. A. Kaharaman 1992 *Nonlinear Dynamics* **3**, 183–198. On the response of a preloaded mechanical oscillator with a clearance: period-doubling and chaos.
16. P. V. Bayly and L. N. Virgin 1993 *Journal of Sound and Vibration* **164**, 364–374. An experimental study of an impacting pendulum.
17. A. P. Ivanov 1994 *Journal of Sound and Vibration* **178**, 361–378. Impact oscillations: linear theory of stability and bifurcations.
18. W. Fang and J. A. Wickert 1994 *Journal of Sound and Vibration* **170**, 397–409. Response of a periodically driven impact oscillator.
19. C. Budd, F. Dux and A. Cliffe 1995 *Journal of Sound and Vibration* **184**, 475–502. The effect of frequency and clearance variations on single-degree-of-freedom impact oscillators.
20. C. J. Budd and A. G. Lee 1996 *Proceedings of the Royal Society of London A* **452**, 2719–2750. Double impact orbits of periodically forced impact oscillators.

21. J. P. Den Hartog 1931 *Transactions of the American Society of Mechanical Engineers APM* **53–9**, 107–115. Forced vibrations with combined Coulomb and viscous friction.
22. E. S. Levitan 1960 *Journal of the Acoustical Society of America* **32**, 1265–1269. Forced oscillation of a spring–mass system having combined Coulomb and viscous damping.
23. M. S. Hundal 1979 *Journal of Sound and Vibration* **64**, 371–378. Response of a base excited system with Coulomb and viscous friction.
24. T. K. Pratt and R. Williams 1981 *Journal of Sound and Vibration* **74**, 531–542. Non-linear analysis of stick/slip motion.
25. D. Tabor 1981 *Journal of Lubrication Technology* **103**, 169–179. Friction: the present state of our understanding.
26. J. R. Rice and A. L. Ruina 1983 *Journal of Applied Mechanics* **50**, 343–349. Stability of steady frictional slipping.
27. E. Marui and S. Kato 1984 *Journal of Dynamic Systems, Measurement and Control* **106**, 280–285. Forced vibration of a base-excited single-degree-of-freedom system with Coulomb friction.
28. R. Parnes 1984 *Journal of Sound and Vibration* **94**, 469–482. Response of an oscillator to a ground motion with Coulomb friction slippage.
29. A. A. Ferri and E. H. Dowell 1985 *Journal of Sound and Vibration* **101**, 55–74. The behavior of a linear, damped modal system with a non-linear spring–mass–dry friction damper system attached, part II.
30. J. T. Oden and J. A. C. Martins 1985 *Computer Methods in Applied Mechanics and Engineering* **52**, 527–634. Models and computational methods for dynamic friction phenomena.
31. S. W. Shaw 1986 *Journal of Sound and Vibration* **108**, 305–325. On the dynamic response of a system with dry friction.
32. R. Greif, B. Schwarz and H. Weinstock 1990 *Journal of Vibration and Acoustics* **112**, 427–428. Resonant response of a system with Coulomb friction.
33. K. Popp and P. Stelter 1990 *Philosophical Transactions of the Royal Society of London. A* **332**, 89–105. Stick-slip vibrations and chaos.
34. P. Stelter and W. Sextro 1991 *International Series of Numerical Mathematics* **97**, 343–347. Bifurcations in dynamic systems with dry friction.
35. P. Stelter 1992 *Nonlinear Dynamics* **3**, 329–345. Nonlinear vibrations of structures induced by dry friction.
36. J. Wojewoda, T. Kapitaniak, R. Barron and J. Brindley 1993 *Chaos, Solitons and Fractals* **3**, 35–46. Complex behavior of a quasiperiodically forced experimental system with dry friction.
37. B. Armstrong-Helouvry, P. Dupont and C. Canudas de Wit 1994 *Applied Mechanics Reviews* **47**, 275–305. Friction in servo machines: analysis and control methods.
38. B. Feeny and F. C. Moon 1994 *Journal of Sound and Vibration* **170**, 303–323. Chaos in a forced dry-friction oscillator: experiments and numerical modeling.
39. D. P. Hess and N. J. Wagh 1994 *Journal of Vibration and Acoustics* **116**, 474–479. Chaotic normal vibrations and friction at mechanical joints with nonlinear elastic properties.
40. R. A. Ibrahim 1994 *Applied Mechanics Review* **47**, 209–253. Friction-induced vibration, chatter, squeal, and chaos. Parts I and II.
41. Y. S. Unlusoy and S. T. Turner 1994 *Journal of Sound and Vibration* **169**, 395–407. Nonlinear dynamic model and its solution for a high speed cam mechanism with Coulomb friction.
42. D. S. Larson and A. Fafitis 1995 *Journal of Engineering Mechanics* **121**, 289–298. Slip-stick steady-state solution for simple Coulomb-damped mass.
43. W. M. Mansour and D. R. Teixeira Filho 1974 *Journal of Sound and Vibration* **33**, 247–265. Impact dampers with Coulomb friction.
44. C. N. Bapat 1995 *Journal of Sound and Vibration* **184**, 417–427. The general motion of an inclined impact damper with friction.
45. G. S. Whiston 1983 *Journal of Sound and Vibration* **86**, 557–562. An analytical model of two-dimensional impact/sliding response to harmonic excitation.
46. C. H. Glocker and F. Pfeiffer 1992 *Nonlinear Dynamics* **3**, 245–259. Dynamical systems with unilateral contacts.
47. K. M. Cone and R. I. Zadoks 1995 *Journal of Sound and Vibration* **188**, 659–683. A numerical study of an impact oscillator with the addition of dry friction.
48. F. F. Ehrich 1990 *Journal of Vibration and Acoustics* **113**, 50–57. Some observations of chaotic vibration phenomena in high speed rotordynamics.
49. D. B. Moore and S. W. Shaw 1990 *International Journal of Non-Linear Mechanics* **25**, 1–16. The experimental response of an impacting pendulum system.

50. K. KARAGIANNIS and F. PFEIFFER 1991 *Nonlinear Dynamics* **2**, 367–387. Theoretical and experimental investigations of gear-rattling.
51. C. N. BAPAT, N. POPPLEWELL and K. MCLACHLAN 1983 *Journal of Sound and Vibration* **87**, 19–40. Stable periodic motions of an impact-pair.
52. N. HINRICHS, M. OESTREICH and K. POPP 1997 *Chaos*, *Solitons and Fractals* **8**, 535–558. Dynamics of oscillators with impact and friction.
53. C. J. BEGLEY and L. N. VIRGIN 1997 *ASME Journal of Dynamic Systems*, *Measurement and Control* **119**, 491–497. A detailed study of the low-frequency periodic behavior of a dry friction oscillator. In preparation.
54. C. J. BEGLEY and L. N. VIRGIN 1997 Grazing and basins of attraction in an impact–friction oscillator, in preparation.
55. M. HENON 1982 *PhysicaD* **5**, 412–414. On the numerical computation of Poincaré maps.
56. H. J. KLEPP 1993 *Mechanics of Structures and Machines* **21**, 357–374. Equivalent viscous damping for systems with friction-affected constraints.
57. L. N. VIRGIN, M. D. TODD, C. J. BEGLEY, S. T. TRICKEY and E. H. DOWELL 1998 *International Journal of Bifurcation and Chaos*. Basins of attraction in experimental nonlinear oscillators,
58. C. J. BEGLEY 1996 *PhD Dissertation*, *Duke University*. The Nonlinear dynamics of an impact oscillator with friction: theory and experiment.
59. B. F. FEENY and J. W. LIANG 1996 *Journal of Sound and Vibration* **195**, 149–154. A decrement method for the simultaneous estimation of Coulomb and viscous friction.
60. A. B. NORDMARK 1991 *Journal of Sound and Vibration* **145**, 279–297. Non-periodic motion caused by grazing incidence in an impact oscillator.
61. H. Y. HU 1995 *Journal of Sound and Vibration* **187**, 485–493. Detection of grazing orbits and incident bifurcations of a forced continuous, piecewise-linear oscillator.
62. F. CASAS, W. CHIN, C. GREBOGI and E. OTT 1996 *Physical Review E* **53**, 134–139. Universal grazing bifurcations in impact oscillators.